Ouzo phase occurrence with alternating lipo/hydrophilic copolymers in water

Henrique Trevisan, Kana Nishimori, Stefano Aime, Jean-Michel Guigner, Makoto Ouchi, Francois Tournilhac

Ouzo phase occurrence with alternated lipo/hydrophilic copolymers in water

Henrique Trevisan,[a] Kana Nishimori,[b] Stefano Aime,[a] Jean-Michel Guigner,[c] Makoto Ouchi[b] and Francois Tournilhac*[a]

Accepted manuscript

Published in

Soft Matter 2021, 17, 7384 - 7395, DOI:10.1039/D1SM00575H

Selection of monomer couples, ensuring reactivity ratios close to zero, is an effective strategy to induce spontaneous copolymerization into an alternated sequence. In addition, monomer design and customisation of the solvent-monomer interactions opens the way to functional copolymers showing molecular self-assembly relevant to their regular amphipathic structure. In this work, we show that the design of comonomers with adequate reactivities and interactions can be used to direct copolymer self-assembly on a mesoscopic scale. We investigate spontaneous formation of nanoparticles through solvent/non-solvent interaction using the so-called "ouzo effect". In this way, an ouzo diagram was built to determine the operation window for the self-assembly, in aqueous suspensions, of alternated copolymers consisting of vinyl phenol and maleimide units carrying long alkyl-pendant groups ($C_{12}H_{25}$ or $C_{18}H_{37}$). Also, investigations were pursued to account for the influence of the lateral lipophilic pendant units on the size and structure of the nanoaggregates formed during one-shot water addition. Structure characterisation by light scattering techniques (DLS and SLS), small-angle neutron scattering (SANS) and transmission electron microscopy (Cryo-TEM and TEM) confirmed the self-assembly of copolymer chains into nanoparticles (size range: 60 – 300 nm), the size of which is affected by the lipophilicity of the alternating copolymers, solvent-water affinity and the solvent diffusion in water. Altogether, we present here the spontaneous ouzo effect as a simple method to produce stable alternating copolymer nanoparticles in water without the addition of stabilizing agents.

Introduction

Preparation of alternating copolymers is a spotlight in the field of polymer chemistry and nanoscience.[1–5] Inspired by natural sequence-regulated systems such as proteins and DNA, these alternating copolymers afford unique self-assembly behaviours.[6,7] The regular alternation of comonomers in copolymer chains allows the spontaneous assembly in organic/aqueous solutions or suspensions to optimise supramolecular interactions.[8,9] During this process, multiple self-assembled structures can be achieved by playing with the design of the copolymer backbone and applying specific solubilisation and/or precipitation methods.[6,10–13]

By doing so, it is possible to prepare aggregate architectures such as spherical micelles, vesicles, wormlike objects, rods, cylinders and lamellar structures that have vast applications in domains as biomedicine and pharmacy, bioimaging, food industry, electronics and sensing.[6,14,15]

To date, two strategies have been identified to produce sequence-controlled alternating copolymers through upscalable processes: i) the cyclopolymerization of divinyl monomers and ii) the design of monomer couples that show reactivity ratios equal to zero, thus opening a connection between precision polymerization and materials science.

Following the first strategy, spontaneous formation of smectic layers was observed for alternating copolymers made of hydrophilic/hydrophobic acrylamide units, whereas random copolymers of same composition remained amorphous.[7] Following the second strategy, a representative case of self-assembly of alternating copolymers is the vermicular core-shell nano-object, established through segregation of hydrogen bond-based phenolic core from alkyl shell in the sequence-controlled AB-alternating copolymer comprising vinyl phenol (A) and n-alkyl maleimide (B) units, reported by Nishimori *et al*.[16] The ordered aggregates are formed upon cooling a solution of the copolymer in aromatic solvents initially at temperatures above 80 °C. Once the mixture is cooled to room temperature, the chain-pendant alternating copolymers arrange themselves giving rise to cylindrical core-shell nano-objects; in a way that solvophobic phenol units are placed in the core, whereas the alkyl side chains are located in the shell pointing towards the solvent continuous phase. Giving sequence to this previous work, our goal is now to investigate the spontaneous assembly of these copolymers in water during solvent-shifting process.

In the aforementioned work, the authors have also shown that the AB-alternating copolymers are soluble at room temperature in several water-miscible solvents such as THF and acetone, but yet, insoluble in water.[16] In fact, this situation fulfils the compulsory condition of spontaneous nanoparticle formation through the so-called solvent-shifting process (also typically referred as “ouzo effect” or non-solvent addition).[11,17–19] The ouzo effect takes its name from the phenomenon

[a] *Molecular, Macromolecular Chemistry, and Materials, CNRS, UMR 7167, ESPCI Paris, PSL Research University, 10 rue Vauquelin, 75005 Paris, France. E-mail: francois.tournilhac@espci.fr*

[b] *Department of Polymer Chemistry, Graduate School of Engineering, Kyoto University, Katsura Nishikyo-ku, Kyoto 615-8510, Japan.*

[c] *Institut de Minéralogie, de Physique des Matériaux et de Cosmochimie, Sorbonne Université, CNRS, UMR 7590, IRD, MNHN, 4 place Jussieu, F-75005 Paris, France.*

Electronic Supplementary Information (ESI) available: [details of any supplementary information available should be included here]. See DOI: 10.1039/x0xx00000x

observed whenever anethol-flavoured drinks such as pastis, ouzo etc., are diluted in water.[18] It also occurs with other molecules and polymers, if the above condition is fulfilled. Amphiphilicity of anethol-like molecules or polymers is the key parameter for this condition to appear. In this regard, an alternating copolymer structure is advantageous because it makes it possible to adjust the amphiphilicity and maintain it constant throughout the chain.

Emulsification through the ouzo effect is straightforward, relying on two plain steps: first, the solute is dissolved in a water-miscible solvent and later on, a large amount of water is rapidly poured in the solution. This causes local chain supersaturation and phase separation into small aggregates and a continuous aqueous phase of turbid aspect.[20] Kinetic features of dilution, related to the interdiffusion of water and solvent molecules are the second key parameter in determining the structure of the colloidal suspension.[11,21]

Typically, thanks to its simplicity, emulsification *via* solvent-shifting has been reported as an advantage to ultrasonication, high-pressure homogenization and other high-shear rate techniques to prepare polymer nanostructures in water.[11,20] This method is also of great interest for preparation of nanocarriers for drug vectorisation and for entrapping water-dispersed solutes to achieve better dispersions without the use of stabilisers.[11,22] In addition, the method is preferably chosen for enabling the preparation of polymer nanoparticles without the need for complicated purification steps, for its low-cost and easy up-scaling.[11] However, this technique has also some obstacles such as the limited range of final polymer mass fraction that leads to ouzo formation (typically from 10^{-5} to 10^{-2}).[17,20,23] This range is commonly referred as "ouzo region" and it is crucial to outline its boundaries to optimise experimental conditions to prepare polymer nanoparticles.

The ouzo composition map was introduced by Vitale and Katz for the *nucleation-and-growth* process of emulsions.[18] This map is the representation of a three-component phase diagram in a bidimensional graph knowing that the mass fraction of the third component is found by difference. The ouzo diagram is characterised by two important boundaries: the equilibrium solubility limit (known as binodal line) and the ouzo stability limit. The binodal line separates the one-phase region (solution) from the metastable colloidal ouzo domain.[20,24] The ouzo limit is the borderline that separates the ouzo range from a second two-phase region, where solvent displacement produces both nano and microparticles aggregates.[17,25]

In fact, one can relate the ouzo effect of polymer in solutions to the phase separation process of polymer mixtures showing an upper critical solution temperature (UCST), in which the decrease of temperature brings the one-phase mixture to the coexistence binodal curve that separates the one-phase region from a metastable domain where nucleation begins.[18,26,27]

By analogy, the addition of water in the ouzo effect corresponds to the effect of temperature decrease in polymer mixtures showing UCST behaviour. Then, the processes differ because stabilization only exists through the ouzo effect once bicarbonate anions adsorb on the interface to render a double layer repulsion and prevent interparticle coalescence.[28] During water addition, the mixing process leads to polymer partition and supersaturation in the aqueous phase, thus polymer solubility and solvent selection is fundamental for this nanoprecipitation technique. Besides, previous works have also shown that preparation variables such as the solvent to non-solvent ratio and the initial polymer concentration influence the properties of the assembled nanoparticles.[23]

Therefore, in this work, we investigate how the alternating copolymers based on vinyl phenol and n-alkyl (alkyl: $-C_{12}H_{25}$ and $-C_{18}H_{37}$) maleimide units spontaneously assemble in water/solvent mixture during solvent-shifting process to prepare polymer nanostructures in aqueous suspension. In this regard, an ouzo diagram is depicted for the two sets of long alkyl chain-pendant alternating copolymers in THF/H_2O mixture. In addition, size features are evaluated with initial copolymer concentration and organic solvent selection. The morphology of the nanoaggregates is also rationalised by dynamic (DLS) and static (SLS) light scattering, small-angle neutron scattering (SANS) and transmission electron microscopy (cryo-TEM and TEM). As far as we know, this work is the first to elucidate the ouzo effect with sequence-controlled copolymers, thus we expect that it will contribute to the advancement of polymer nanoparticle preparation *via* the ouzo effect.

Experimental

Materials

The preparation of the copolymers used here [poly(4-vinylphenol-*alt*-dodecylmaleimide) M_n= 88,000 and M_w/M_n= 6.61, AltC12] and [poly(4-vinylphenol-*alt*-octadecylmaleimide) M_n= 209,600 and M_w/M_n= 2.41, AltC18] has been reported in a previous work. The synthesis involves protection of the hydroxide function, free radical copolymerization of *p-tert*-butoxy styrene (M_1) and *n*-alkyl maleimide (M_2), followed by a deprotection step. The intensity of characteristic ^{1}HNMR signals of both comonomers was used to determine their relative abundance in the copolymer, where it was found close to 50/50 mol% regardless of the co-monomer feed ratio. Fitting the results indicated reactivity ratios close to zero (r_1 = 0.017 and r_2 = 0.000).[16]

For the preparation of the nanoparticles, the solvents THF, 1,4-dioxane and acetone (Aldrich; purity >99%) and the non-solvent (water, ASTM type 1) were filtered before use in hydrophilic syringe filters of 0.2 µm, (Pall Corporation, USA).

Nanoparticle preparation and construction ouzo phase diagram

For the preparation of the metastable copolymer nanoparticles, stock solutions (1 – 20 mg mL^{-1}) of AltC12 and AltC18 were first prepared with water-miscible organic solvents (THF, acetone or dioxane) and they were left to equilibrate for 12h. In sequence, type 1 water was rapidly poured to each stock solution respecting the copolymer solution to water volume ratio of 1:5 (v/v). The phenomenon of spontaneous emulsification (ouzo effect) is observed instantly with the emergence of a slightly turbid suspension.

To build the phase diagram, amounts of organic solvent (THF), copolymer and water were chosen to reach the desired

final mass fractions in the ternary system AltC12 (or AltC18)/THF/H_2O. For simplicity, the masses were measured with an analytical balance (Sartorius SECURA 224-1s, +/- 0.1 mg) during ouzo preparation. For instance, to prepare a suspension with copolymer mass fraction of 1.7 x 10^{-4}, 1 mg of copolymer is dissolved in 0.889 g of THF (ρ_{THF} = 0.889 g mL^{-1} at 25 °C) and, afterwards, 4.99 g of water (ρ_{water} = 0.997 g mL^{-1} at 25 °C) is poured into the solution. This procedure is followed for all suspensions that were prepared with copolymer mass fractions from 1.0 x 10^{-4} to 1.0 x 10^{-3}.

Binodal line determination

The binodal line was determined following a procedure adapted from literature, which consists of a 'reverse' titration-like technique.[17] First, ouzo suspensions were prepared with increasing copolymer mass fractions (10^{-4} to 10^{-3}) and their initial light scattering intensities (I_0) were measured with a standard light scattering equipment with goniometer setup (single angle used, 90°) (ALV/LSE – 5004, λ 633 nm, Langen, Germany). Afterwards, sequential amounts of THF were added to each colloidal suspension (magnetically stirred, 400 rpm) with the aid of a syringe pump (Harvard Apparatus, pump 33DDS 0.5 µL +/- 0.25%) connected to the vial containing the suspension and closed with a rubber septum to avoid solvent evaporation. After each solvent addition, the light scattering intensity (I_f) of the suspension was measured and the normalized scattering intensity $NI = I_f/I_0$ was plotted as a function of the mass of THF added to the system (Fig. S1 and Fig. S4). It was thus possible to determine the amount of THF needed to dissolve the copolymer in the solvent/non-solvent mixture by using the method of tangents. Considering that the mass of copolymer and water did not vary during the THF titration, the mass fractions can be calculated knowing that $f_{water} + f_{copolymer} + f_{THF} = 1$. The result is plotted in (Fig. S2 and Fig. S5).

The binodal line for AltC12 was also determined following a direct titration *via* water addition to copolymer solutions in THF (mass fractions from 10^{-4} to 10^{-3}), Fig. S3. The binodal line thus determined is less accidented, but the absolute position of the transition is shifted upwards probably because visual detection of the transition is biased by transient appearance of turbidity at each drop when approaching the actual transition. Therefore, the 'reverse' technique was chosen for binodal line determination because while doing so, the initial ouzo phase (taken as starting point in measurement) is always prepared by the same protocol and its structure is verifiable by dynamic light scattering.

Ouzo-stability line determination

For the stability-limit curve determination, different ouzo suspensions were prepared as previously mentioned with fixed initial copolymer mass fraction (5.0 x 10^{-4}) and increasing THF initial mass fractions (0.10; 0.15; 0.20; 0.25 and 0.30). The optical density ($Abs_{initial}$ at λ = 600 nm) of these suspensions was measured with a UV-VIS Spectrophotometer (Shimadzu UV-2401 PC). Afterwards, a solution of each copolymer (AltC12 or AltC18) in THF (25 mg mL^{-1}) was added progressively to the respective copolymer nanoparticle suspension with the aid of a syringe pump and, after each addition under magnetic stirring, the absorption (Abs_{final} at λ = 600 nm) of the resulting suspension was measured. By plotting the absorbance ratio ($Abs_{final}/Abs_{initial}$) as a function of the mass fraction of the copolymer and THF added to the system, it was possible to determine the ouzo limit (Fig. S6 and Fig. S7). This limit is characterised by a sharp decrease of the absorbance ratio once macroscopic phase separation occurs, which is defined by the agglomeration of nanoparticles and separation from the bulk of the suspension. Considering that the masses did not vary during the analysis, the mass fractions can be calculated knowing that $f_{water} + f_{copolymer} + f_{THF} = 1$.

Characterisation of nanoparticles

All characterisations were performed on as-prepared samples, meaning that a mixture of copolymer/solvent/non-solvent is present. TEM is the only exception where samples were dried.

Dynamic Light Scattering (DLS) and Static Light Scattering (SLS). A standard light scattering equipment with goniometer setup from ALV/LSE – 5004, Langen, Germany was used to obtain both the hydrodynamic radius (R_H) and the radius of gyration (Rg) of the copolymer self-assembled nanostructures in aqueous dispersion at 20 °C. For DLS experiments, the suspension was transferred to a glass tube (Φ 10.00 mm) and the scattered intensity I (q,t) was monitored at 90° with three runs of 90 s each. The raw data was converted to the time intensity correlation function using the hardware correlator ALV – 7004. The Cumulants method was used to fit experimental data points and to calculate the translational diffusion coefficient and the hydrodynamic radius (R_H) by using Stokes-Einstein equation.[29]

For the SLS experiments, the absolute scattering intensity (so-called Rayleigh ratio, R) was determined from the measured scattered intensities of the dispersion (I_{dis}) and the non-solvent (water) (I_w) as well as from the intensity of toluene (I_{tol}) as scattering standard. The q^2 -range was covered from 6.85 x 10^6 to 2.55 x 10^7 m^{-2} and the Rayleigh ratio was calculated as given in Eq. 1; where n_w and n_{tol} are the refraction indexes of water (1) and toluene (1.49) respectively, and R_{tol} is the Rayleigh ratio of toluene (1.3522 x 10^{-5} cm^{-1} at 633 nm). In addition, the scattered intensities were normalized by factorisation with sinθ as given in Eq. 2, where I_{scat} is the measured scattering intensity, I_{mon} is the intensity of the incident beam light and θ is the scattering angle (from 30° to 150° with angular step of 2°). The radius of gyration (Rg) was determined from the graphical representations of R vs q using the shape-independent Guinier-Porod fitting model on SasView software.[30]

$$R(cm^{-1}) = \frac{I_{dis} - I_w}{I_{tol}} \left(\frac{n_w}{n_{tol}}\right)^2 R_{tol} \quad (Eq.1)$$

$$I(q,t) = \frac{I_{scat}}{I_{mon}} \sin\theta \quad (Eq.2)$$

The absolute scattering intensity was fitted in both low and high – q range assuming the Guinier (Eq.3a) and Porod (Eq. 3b) contributions; where Rg is the radius of gyration, d is the Porod exponent and G and D are the Guinier and Porod scale factors,

respectively.

Table 1 Sample list of copolymer suspensions (AltC12 and AltC18) and respective used solvents and non-solvent for SANS experiments. For comparison, only copolymer solutions in THF and THF-*d*8 were prepared. The scattering length densities (SLD) of each pure component and the incoherent background of SANS data are also listed.

Sample	Non-solvent	SLD Copolymer x10^{10}(cm^{-2})	SLD solvent x10^{10}(cm^{-2})	SLD non-solvent x10^{10}(cm^{-2})	Incoherent background level (cm^{-1})
D_2O	-	-	-	6.33	0.04
AltC12/D8	D_2O	0.75	6.35	6.33	0.04
AltC12/H8	D_2O	0.75	0.18	6.33	0.11
AltC18/D8	D_2O	0.54	6.35	6.33	0.04
AltC18/H8	D_2O	0.54	0.18	6.33	0.11

D8=THF-*d*8; H8=THF

$$I(q) = G\ exp\left(\frac{-q^2 R_g^2}{3}\right); for\ low\ q-range\ (Eq.3a)$$

$$I(q) = \frac{D}{q^d}; for\ high\ q-range \quad (Eq.3b)$$

$$\text{where, } D = G \exp\left(\frac{-d}{2}\right)\left(\frac{3d}{2}\right)^{d/2}\frac{1}{R_g^d}$$

Small-Angle Neutron Scattering (SANS). SANS experiments were performed on line D22 at the Institute Laue Langevin in Grenoble, France.[31] The incident radiation was monochromatic (λ = 6 Å) and sample-to-detector distances D = 1.5 m, 5.6 m and 17.6 m were used. Additionally, D = 17.6 m was used at λ = 11.5 Å thus covering a q-range from 0.001 Å^{-1} to 0.55 Å^{-1}. Samples were prepared as described previously, starting from solutions in THF, with constant final mass fractions of $f_{copolymer}$= 4.5 x 10^{-4} and $f_{solvent}$= 0.082. The copolymer suspensions were also prepared in the deuterated solvent for contrast variation as indicated in Table 1.[32] Finally, the suspensions were transferred to amorphous silica (quartz) Hellma cells (optical path: 1 mm, cell volume = 300 µL) for analysis at 25 °C.

For AltC12 suspensions reduced SANS data were corrected from incoherent scattering background and the radius of the spherical particles was deduced using the Porod's limit, as described by Isabelle Grillo.[33] In this sense, the specific surface area Σ (cm^2 cm^{-3}) was calculated as indicated on Eq. 4; where Δρ is the difference of scattering length densities (SLD) between the copolymer particles and the non-solvent/solvent mixture (weighted arithmetic mean); I(q) is the scattered intensity on absolute scale (cm^{-1}) and q is the module of scattering vector.

$$\sum (cm)^2/(cm)^3 = \frac{1}{2\pi(\Delta\rho)^2}\lim_{q\to\infty} I(q)q^4 \quad (Eq.4)$$

Assuming the spherical geometry of the copolymer nanoparticles and neglecting their polydispersity, the radius (R) can be estimated from the specific surface area (Σ) and the mass fraction (Φ) as indicated on Eq. 5

$$R = \frac{3\Phi}{\Sigma} \quad (Eq.5)$$

For AltC18 scattering curves, the two data sets (with deuterated and non-deuterated solvent) were fitted together in a constrained mode, requiring the radii to be identical and only the SLDs to differ between the two data sets. A constrained core-shell model fitting was thereby done using the SasView software[34] to estimate the shell-thickness and the radius of the nanoparticles; assuming a neat AltC18 shell and a core of entrapped copolymer chains and solvent mixture. This model best described the profile of the AltC18 SANS curves with contrast variation.

The core-shell model used to fit the scattering data is given on Eq. 6

$$I(q) = \frac{N}{V}|b(q)|^2 \quad (Eq.6)$$

Where, *N/V* is the number of particles per unit of volume and *b(q)* is the scattering length of the particle (see supplementary information), as given on Eq. 7

$$b(q) = 3V_s(\rho_{shell} - \rho_{solvent})\frac{sin(qr_s) - qr_s\,cos(qr_s)}{(qr_s)^3}$$

$$+ 3V_c(\rho_{core} - \rho_{shell})\frac{sin(qr_c) - qr_c\,cos(qr_c)}{(qr_c)^3} \quad (Eq.7)$$

Where, V_C and V_S are the volume of the core and the total volume of the particle; r_c and r_S are the radius of the core and of the outer shell; ρ_{core}, ρ_{shell} and $\rho_{solvent}$ are the scattering length densities of the core, of the shell and of the solvent, respectively.

Cryo-Transmission (Cryo-TEM) and Transmission Electron Microscopies (TEM). The morphologies of the copolymer nanoparticles were examined using a LaB6 JEOL JEM 2100 transmission electron microscope operated at 200 kV with a minimum dose system, MDS. For Cryo-TEM sample preparation, the dispersions ($f_{copolymer}$= 4.5 x 10^{-4}; in copolymer/THF/H_2O mixture) were pipetted (5µL droplet) on a Quantifoil holey-carbon-coated grid (Quantifoil Micro Tools) and rapidly frozen by plunging the grid into liquid ethane. Images were recorded with an Ultrascan 2k × 2k CCD Gatan camera. For TEM analysis the samples were pipetted on carbon-coated Cu grids (CF400-Cu, Electron Microscopy Sciences) and dried overnight in desiccator.

Results and discussion

In the previous work, it was shown that by strategic selection of comonomers it is possible to prepare sequence-controlled copolymers simply *via* radical copolymerization,

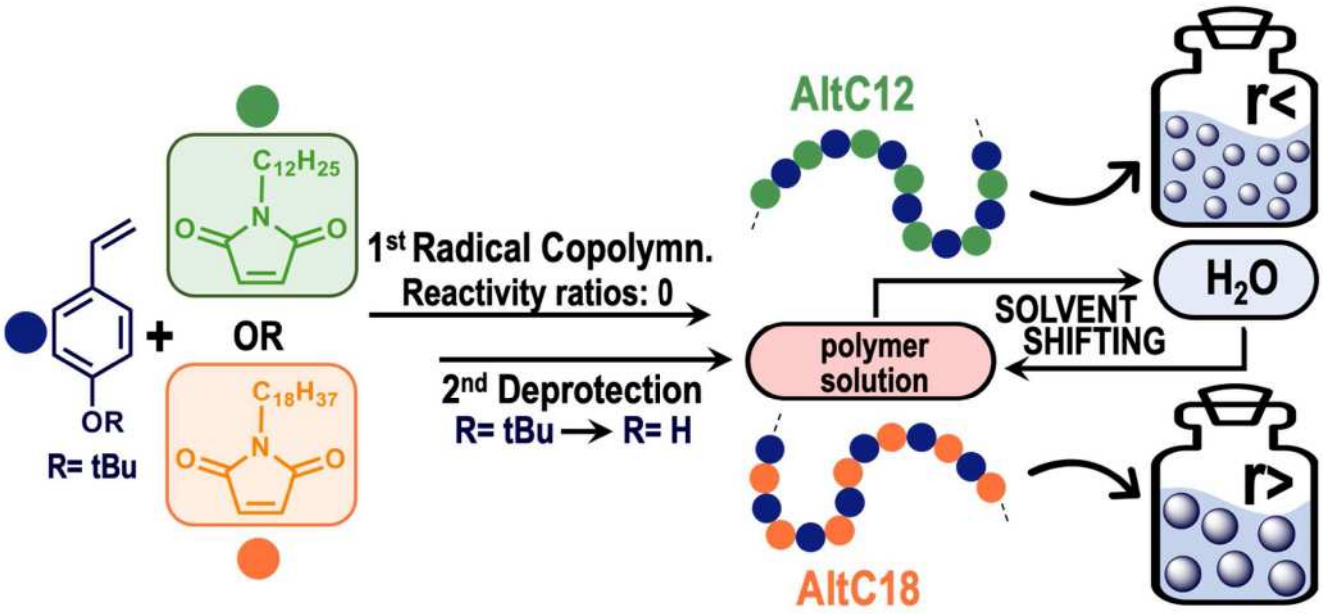

Fig. 1 Alternating copolymers consisting of vinyl phenol and alkyl-pendant maleimide units (AltC12, green, for alkyl = $C_{12}H_{25}$ and AltC18, orange, for alkyl = $C_{18}H_{37}$) were prepared in a previous work (see reference 16) *via* radical copolymerization and subsequential deprotection of the styrene substituent. In this work, polymer nanoparticles were prepared from solutions of the copolymers in a water-miscible solvent via solvent-shifting process "ouzo effect". AltC18 is more lipophilic than AltC12 and leads to formation of bigger nanoparticles.

since the reactivity ratio of the comonomer pair *p*-tert-butoxystyrene and N-alkyl maleimide is close to zero, which means that each active monomer species will favour its comonomer pair leading to a spontaneous cross-over propagation reaction.[16] In this present work, we show that by controlling the number of carbons in the alkyl-pendant maleimide unit and, thus, tuning the lateral lipophilicity of the copolymer chain, it is possible to prepare polymer nanoparticles with different sizes and structures as a result of the extent of intermolecular interactions and solvent diffusivity in water during the "ouzo" solvent-shifting process (Fig. 1).

In the next sections, we present the domain of occurrence of the ouzo phase as well as the characterisation of the nanostructures that are formed. Thus, the use of the solvent-shifting process to produce nanoparticles from AB sequence-controlled copolymers is proposed. We also show that previous knowledge on the nature of nanoprecipitation is applicable to elucidate the physicochemical cause for the self-assembly process of the copolymer chains during supersaturation and solvent diffusion in water. [2,11,20]

Domain of occurrence of the ouzo phase: binodal and ouzo limit boundaries

It is important to depict the composition window of solvent/copolymer/H_2O that leads to the self-assembly of macromolecules into nanoparticles, mostly for further applications that require specific colloidal formulations and to elucidate the ouzo effect for the class of AB-alternating copolymers that we are investigating herein. Therefore, an ouzo diagram was derived rather than following a "trial and error" approach to determine the operating window for nanoparticles assembly. The ouzo region is delimited by two characteristic borders: the binodal (miscibility limit) and ouzo limit (stability limit) curves. It is within this region where it is possible to induce polymer chains supersaturation during the one-shot water addition to produce metastable nanoparticles.[11,23] By analogy, the topology of the ternary diagram for the anethol/water/ethanol system is shown in Scheme 1. The milky drink is prepared by adding water to the alcoholic solution following path 1 to 2 reaching a final composition within the metastable domain where self-emulsification of anethol occurs.[22,33,35]

It looks very straightforward to prepare a Pastis to serve on a blazing summer day. One thing that one does not realize on this occasion, is that the obtention of the milky colour drink solely happens in a very narrow composition window. In fact, this region can be highlighted if the ternary phase diagram is rather represented in a two-dimensional graph showing the mass fraction of the organic solvent on the ordinate and the

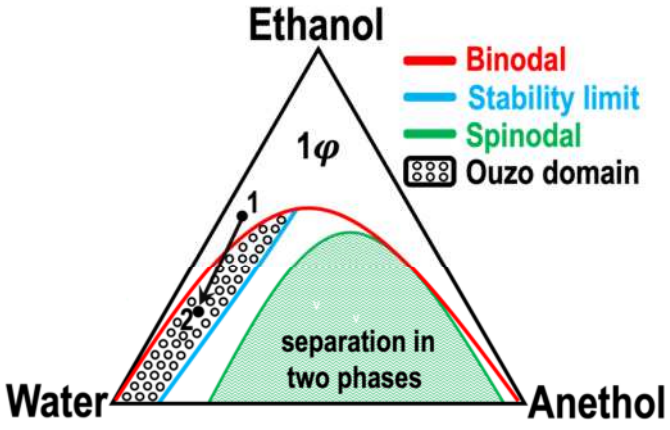

Scheme 1 Topological representation of ternary phase diagram of the system anethol/water/ethanol. The ouzo effect takes place once solutions are brought from the one phase (1ϕ) stable domain region (1) to the narrow metastable domain between binodal and ouzo stability lines (2) by water addition.

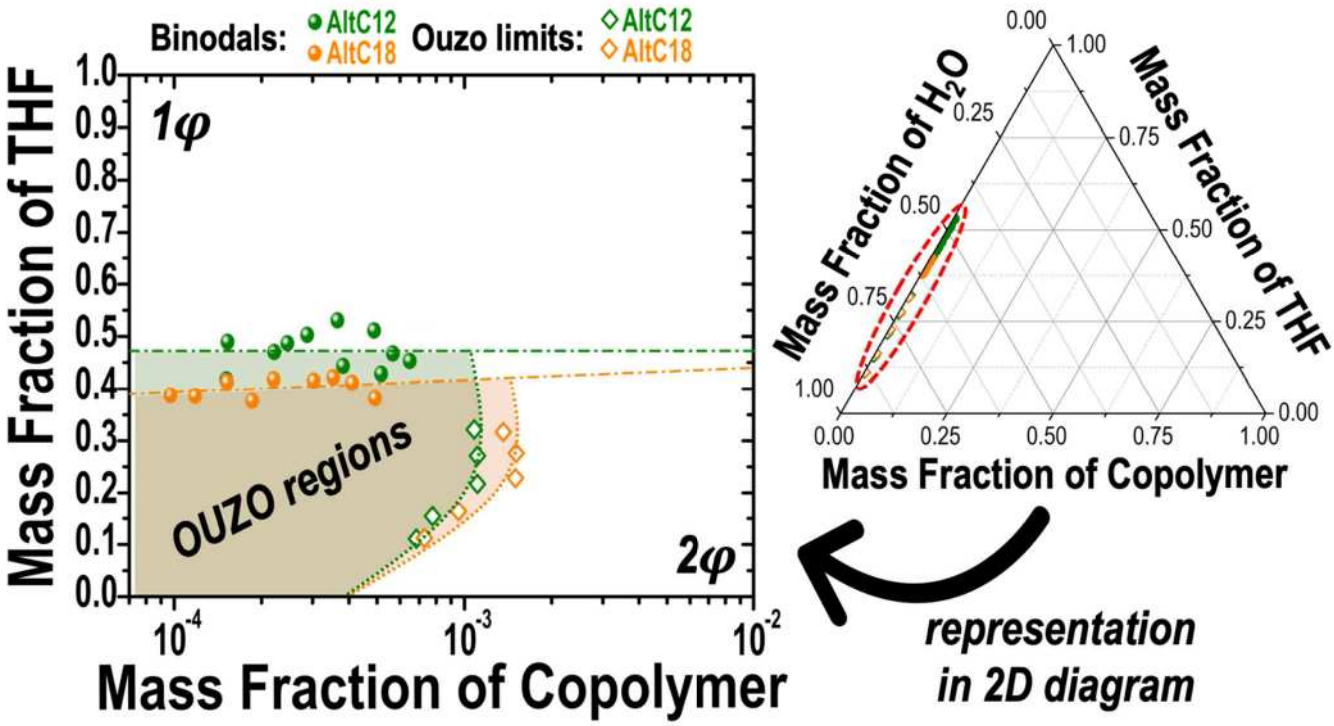

Fig. 2 Ouzo bidimensional phase diagram (P, T= constants) depicting the mass fractions of THF versus the mass fractions of the copolymers (AltC12 and AltC18). The mass fraction of water can be determined from the other two components by subtraction. Copolymer nanoparticles are assembled once the mass fraction of water increases, and the solutions are brought from the one-phase region (1φ) to the metastable ouzo domain between binodal and ouzo limit curves. The miscibility-limit line (binodal) is the best fit of experimental points determined by sequential addition of THF to metastable nanoparticle dispersions and followed by light scattering until solubilisation. The ouzo limit boundary was determined by copolymer addition to ouzo suspensions, in which further increase of copolymer mass fraction leads to formation of macroscopic aggregates (2φ). The ouzo region is represented in a two-dimensional graph, since it is not possible to distinguish this region in a classic ternary plot.

mass fraction of the solute on the abscissa using a log scale.[18] Likewise, Fig. 2 shows the bidimensional ouzo diagram for the alternating copolymers AltC12 and AltC18 in a mixture of THF as solvent and water as non-solvent.

Two important features can be extracted from this diagram: the position of the binodal lines characterised by the miscibility limit of AltC12 and AltC18 in the THF/water mixture and the ouzo stability boundary, where the metastable nanostructures coalesce. Beyond the ouzo limit there is a coexistence of both macroscopic structures, that phase separate from the bulk of the suspension, and nanoparticles that remain in dispersion.[17,24,25]

It is possible to observe that the binodal boundary of AltC18 is below the binodal line of AltC12 (Fig. 2). The explanation for this trend relies on the solvent affinity and the copolymer partition in solvent/water mixture once the supersaturation is reached.[23,36] Since AltC18 is more lipophilic than AltC12, the nanoparticles of the former solubilise easier in the THF/water mixture than the AltC12 ones once the amount of THF increases. In other words, THF is a better solvent to the copolymer with alternating alkyl groups of 18 carbons than it is to the alternating copolymer with 12 carbons in the alkyl-pendant unit. Aubry *et al.* have previously showed that the position of the binodal line also changes depending on the solvent selection (acetone or THF) for nanoparticles prepared from polymethylmethacrylate.[17] Accordingly, we could also expect a shift of the binodal lines for AltC18 and AltC12 in mixtures prepared with other water-miscible solvents than THF.

The self-assembly process in the ouzo region occurs once copolymer solutions are rapidly brought to the region between the binodal and ouzo limit curves by fast water addition.[20] The copolymer chains are spontaneously assembled into nanoparticles during the rapid diffusion of the solvent in water.[23] Moreover, the driving force for the self-assembly process is the magnitude of the entropic gain associated to the release of water molecules from the solvation shell around the macromolecules. This gain is greater than the entropic loss associated with the assembly of the copolymer chains into aggregates – a phenomenon known as hydrophobic effect.[9] However, for large solute concentrations, the nanostructures agglomerate and grow therefore spontaneously yielding macroscopic aggregates in addition to the nanoparticles.[11,25] As shown in Fig. 2, it is possible to see that the ouzo stability line depends both on the mass fractions of THF and the copolymer.

Both ouzo limits showed a characteristic decrease at low mass fractions of copolymer and solvent (Fig.2), similar trend was also observed by Lucas *et al.* for the ouzo limit of PMMA nanoparticles prepared from solution in acetone, it is possible to relate this decrease to the supersaturation process during the non-solvent addition.[36] Since there is lower amount of solvent in the system, local chain supersaturation is easily reached and further increase of AltC12 or AltC18 mass fractions leads to further phase separation. Beyond the ouzo stability

border, there is a coexistence of nanoparticles and flocculate aggregates that are less dense and stick to the walls of the vial, which allowed the determination of the ouzo limit points *via* optical density measurements (Fig. S6 and Fig.S7). In addition, the ouzo diagram shows that AltC18 enables the production of slightly more concentrated nanoparticle suspensions for high THF mass fractions, since the location of its ouzo limit is after the AltC12 stability borderline.

It is well known that the ouzo effect is strictly dependent on the initial polymer mass fraction and on the nature of the solvent that is used.[23] In the present work, we have also verified how the copolymer lipophilicity can be tuned to achieve nanostructures with different sizes. In this sense, in the next section we investigate the structure of the ouzo phase and the relation between size trends, copolymer concentration, solvent-water affinity and solvent diffusivity in water.

Ouzo phase size trends and structure

The mixing process during solvent-shifting by water addition leads to copolymer partition in the solvent/H_2O mixture and the formation of the nanoaggregates — whose size is dependent on the extent of: 1st) solvent/non-solvent interdiffusion; 2nd) solvent-copolymer interaction (copolymer lipophilicity) and 3rd) polymer chain diffusion during ouzo effect, which is governed mainly by the molecular weight of the copolymer.[23,37] In this way, we expect that organic solvents that have higher water-affinity and higher diffusivity will switch rapidly from the copolymer solution to the aqueous medium and lead to faster supersaturation process and, thus, smaller copolymer nanoparticles formation. Here, we also show that the supersaturation process during solvent diffusion can be controlled by the selection of either AltC12 or AltC18, knowing that AltC12 is less lipophilic and this particular sample has lower molecular weight than the AltC18 one.

Dynamic light scattering (DLS) is a useful tool to measure the Brownian motion of particles in suspension and correlate their translational diffusion with the respective hydrodynamic radius (R_H), which gives us a picture of the hydrodynamic size of submicron particles. In Fig. 3a, it is possible to observe the increase of the R_H with the copolymer concentration (increasing AltC12 or AltC18 mass fractions). This trend is associated with the escalating amount of copolymer chains in the medium that are added to the born particle nucleus, which is formed during solvent displacement. By fitting the data in Fig.3a, the slopes of 0.30 (R^2=0.91) for AltC12 and 0.53 (R^2=0.94) for AltC18 are obtained. For AltC12, the slope is close to 1/3, which indicates that the most probable mechanism for the formation of the nanoaggregates is the *nucleation-aggregation* one, thus the volume of the nanoparticles is directly proportional to the copolymer concentration.[17] As for AltC18, the slope is much larger than 1/3, meaning that the volume of the particles is not only dependent on the initial concentration of AltC18 solutions.

This observation may be an indication that AltC18 nanoparticles also entrap solvent during their formation, which could explain the sharp size increase. Another pattern depicted in Fig. 3a is that AltC18 form bigger submicron structures than AltC12 and that is because THF displays better affinity to AltC18 as mentioned previously. This higher solvent affinity to AltC18 leads to a slower supersaturation process during non-solvent addition and, consequently, formation of bigger particles. As for

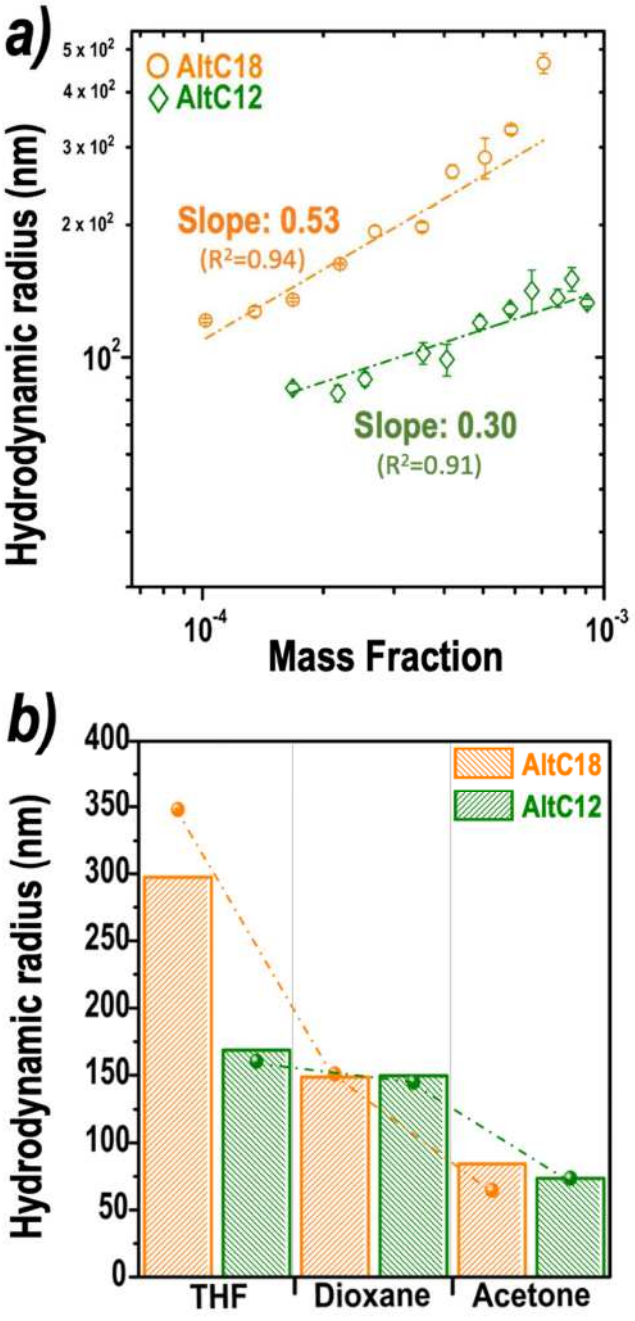

Fig. 3a) Log-Log hydrodynamic size trend with increasing mass fraction of AltC18 and AltC12 (nanoparticles prepared from THF solutions). Horizontal scale relates to final copolymer mass fraction; vertical scale relates to the mean hydrodynamic radius. Error bars are standard deviation from triplicates measured by DLS at 90º scattering angle room temperature (20 °C). **b)** Hydrodynamic size trend of AltC12 and AltC18 nanoparticles (mass fraction = 4.5 x 10^{-4}) prepared from copolymer solutions in THF, Dioxane and Acetone. Bars show the hydrodynamic radius of suspensions freshly prepared and symbols (-●-) show the hydrodynamic radius of respective suspensions after 6 months, stored at room temperature.

AltC12, the solvent diffusion to the aqueous medium is more efficient and leads to smaller colloidal particles.

Likewise, once we prepare these ouzo suspensions using other solvents than THF (dioxane and acetone) it is also possible to observe the dependency of particle size with solvent diffusivity and water-solvent affinity. Fig. 3b shows that, for both copolymers, the size of the assembled nanostructures decreases with the increase of solvent diffusivity in water and water-solvent affinity (indicated by lower interaction parameter, χ value): THF (D=1.09 x 10^{-5} cm^2 s^{-1}; χ=26.1) ≈ dioxane (D=1.11 x 10^{-5} cm^2 s^{-1}; χ=23.3) < acetone (D=1.28 x 10^{-5} cm^2 s^{-1}; χ=13.2).[23,38] Acetone has lower viscosity and higher water affinity than the ether solvents and thus allows faster mixing and uniform supersaturation, which gives nanoparticles with hydrodynamic radii smaller than 100 nm for both AltC12 and AltC18. The nanoparticles prepared with AltC12 follow a size-trend decrease in accordance with the increasing solvent diffusivity and water affinity. However, for AltC18, it is possible to observe that the R_H in THF is approximately the double of the nanoparticles prepared from dioxane solution, this result might be related to the change of the structure and the entrapping of solvent during the nanoparticle formation, as discussed in the next sections.

In addition, as shown in Fig. 3b, the nanostructures prepared by the ouzo effect from copolymer solutions in different organic solvents showed to be remarkably stable over time, since the hydrodynamic radii have not changed considerably after 6 months. This result might be related to colloidal stabilization *via* the adsorption of bicarbonate anions on the surface, which confers electrical double layer repulsion between the nanoparticles, thus hindering interparticle coalescence.[22,28,39] Moreover, these copolymer suspensions are kinetically stable without the addition of any stabilizing agents as surfactants or buffering solutions. This is an important aspect considering the future application of these copolymer nanoparticles to entrap water-dispersed solutes and achieve dispersions without additives.[11,36]

Molecules of interest could be dissolved in the copolymer solution and via the ouzo effect one should be able to induce the encapsulation. By the same token, by preparing a solution or suspension of a product or pigment of interest in water, it may be possible to entrap it in the nanostructures prepared during solvent shifting. For instance, Lucas *et al.* showed that it is possible to entrap carbon nanotubes (dispersed in water) in poly(methylmethacrylate) nanoparticles prepared via ouzo effect for subsequential nanocomposite films preparation.[36]

Characterisation of the nanoparticles by complementary spectroscopic techniques

Using the ouzo effect, Chen *et al.* showed that main chain alternating copolymers prepared *via* epoxy–thiol click reaction between 1,4-butanedithiol and butadiene diepoxide form nanotubes once water is added to their solution in DMSO (solvent-shifting process).[40] By following a different approach, Fenimore *et al.* also reported that alternating copolymers of N-alkylmaleimides and vinyl gluconamide self-assemble into unilamellar vesicles once they are directly dissolved in water (not ouzo effect).[41,42]

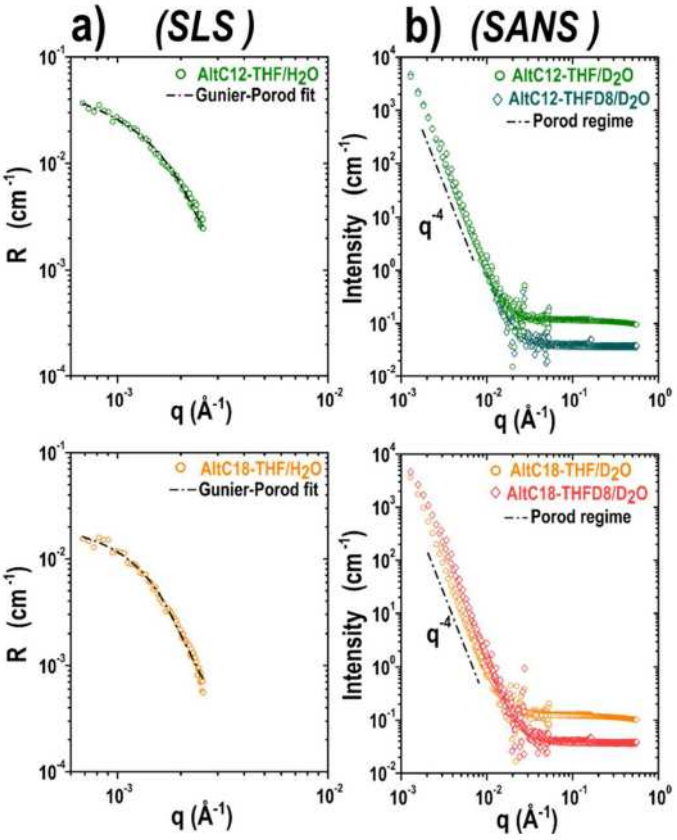

Fig. 4a) Absolute light scattering intensities (R) as a function of the scattering vector measured for the copolymer (AltC12 and AltC18; mass fraction= 4.5 x 10^{-4}) suspensions prepared from solutions in THF *via* fast water addition. The scattered intensities were corrected for the angle dependent scattering volume and measurements were performed at 20 °C. Dashed lines are the Guinier-Porod fitting of experimental points for R_g determination. **4b)** SANS data for copolymer nanoaggregates (AltC12 and AltC18) in THF/D_2O or deuterated THF-*d*8/D_2O obtained at 25 °C. SANS curves exhibit $I \propto q^{-4}$ behaviour characteristic of spherical structures. The Porod regime in the SANS data was used for determination of Porod's limit and radii of the AltC12 nanoparticles (Fig. S8) while the core-shell fitting model best described the AltC18 scattering data (Fig. S9; χ^2= 90 for THFd8/D_2O and χ^2= 217 for THF/D_2O).

Here, we show that the ouzo effect also plays an important role for AltC12 and AltC18 self-assembly. Although, these copolymers have an amphiphilic backbone, they are not soluble in water — for poly(N-alkylmaleimides-alt-vinyl phenol), solubility in water at 1 wt. % would require alkyl chains as short as C_2H_5 and a basic medium.[16] With AltC12 or AltC18, during the rapid water addition and chain supersaturation, fast *nucleation-aggregation* takes place and results on colloidal nanoparticles formation. As shown in Fig. 4a and 4b, we were able to analyse the structure of the nanoparticles by using a combination of static light scattering (SLS) and small-angle neutron scattering (SANS) with contrast variation. The SANS data essentially show the $I \propto q^{-4}$ Porod behaviour, which is characteristic for sharp interfaces, whereas the scarcely detectable curvature relevant to the size of the objects appears more clearly on SLS data.[30] By representing the absolute light scattering (R) versus q it is possible to fit the experimental data using the Guinier-Porod

Table 2 Sizes estimation by SANS, DLS and SLS data recorded at room temperature for AltC12 and AltC18 in THF/H_2O (for light scattering techniques) and THF/D_2O or THF-*d*8/D_2O mixtures (for SANS measurements). The shape factor (ρ - ratio) is determined from the ratio of the radius of gyration (Rg) and the hydrodynamic radius (R_H). The Porod's limit was used to estimate the radius and the scattering length densities (SLD) of AltC12 nanoparticles with contrast variation. The core-shell model was used to fit the AltC18 data to estimate the radius, shell thickness and the SLDs of the core and continuous phase with contrast variation.

Porod's limit	Lim I(q)q^4 x10^{24}(cm^{-5})	SLD particle x10^{10}(cm^{-2})	ΔSLD x10^{10}(cm^{-2})	Specific area Σ (cm^2 cm^{-3})	Radius (in D_2O) by SANS (nm)	R_H (in H_2O) by DLS (nm)	Rg (in H_2O) by SLS (nm)	ρ - ratio (Rg/R_H)
AltC12 – THFD8	1.03	1.30	-5.0	65	210	-	-	-
AltC12 – THF	1.05	0.69	-5.1	65	210	160	100	0.62

Core-shell model	SLD Core x10^{10}(cm^{-2})	SLD Shell x10^{10}(cm^{-2})	SLD Continuous phase x10^{10}(cm^{-2})	Shell thickness (nm)	Radius (in D_2O) by SANS (nm)	R_H (in H_2O) by DLS (nm)	Rg (in H_2O) by SLS (nm)	ρ - ratio (Rg/R_H)
AltC18 – THFD8	5.34	0.54	6.33	130	370	-	-	-
AltC18 – THF	0.93	0.54	5.77	130	370	300	136	0.45

empirical model, which takes into account both Guinier and Porod scale factors (Eq. 3a and 3b). This model has nicely fitted the experimental data giving the Rg values for both AltC12 and AltC18 nanoparticles (Figure 4a; Table 2). The Rg/R_H ratio (ρ – ratio) provides an important indication on the topology of the nanoaggregates assembled *via* ouzo effect.

The theoretical shape factor of nanoparticles with homogeneous internal density is of 0.78 while swelled or core-shell polymer nanoparticles typically show ρ – ratios ranging between 0.4 — 0.6.[29,43,44] Likewise, both AltC12 and AltC18 nanoparticles have shown ρ – ratios close to this range (Table 2). In fact, the shape factor of AltC12 nanoparticles is bigger than the shape factor of AltC18 nanoparticles; this result indicates that the first ones have a denser and slightly swelled inner core. It is possible to relate this information to the fact that AltC18 is more lipophilic than AltC12 and during the solvent displacement process, the solvent does not diffuse easily to the continuous aqueous medium as it does for AltC12 mixture.

The SANS data is in line with the hypothesis that AltC12 nanoparticles are in fact found in a slightly swollen state. As shown in Figure 4b, the neutron scattering data of AltC12 nanoparticles in THF/D_2O and THF-*d*8/D_2O overlap in the q-range between 10^{-3} and 10^{-2} $Å^{-1}$, meaning that the scattering intensity in the Porod region does not change with the contrast variation.[45] Indeed, the calculation of the Porod's limit (Fig. S7) gives values that are similar (Table 2). Therefore, the amount of THF in the swollen nanoparticles can be determined knowing that the specific surface areas of AltC12 nanoparticles in both mixtures are equal (Table 2). This result implies that the scattering length density of AltC12 nanoparticles is of 0.69 x 10^{10} cm^{-2} in the THF/D_2O mixture and 1.30 x 10^{10} cm^{-2} in the THF-*d*8/D_2O mixture, thus comprising 0.55 µL of THF in the swollen nanoparticles.

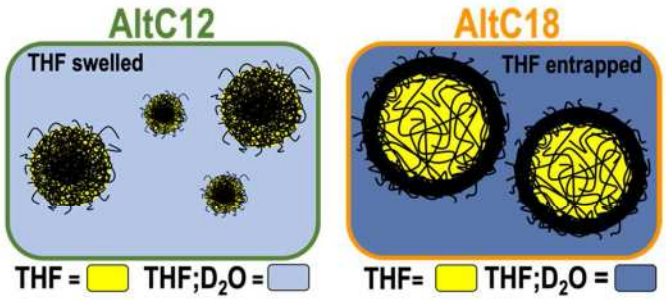

Scheme 2 Illustration of the nanoaggregate structures formed during ouzo effect confirmed by SANS measurements and transmission electron microscopy imaging. AltC12 copolymer chains self-assemble into slightly swollen nanoparticles, while AltC18 copolymer chains form a type of core-shell structures entrapping a solvent /copolymer mixture in the core. Colour scales represent the solvent (THF) and solvent mixtures (THF, D_2O) in the two systems.

Assuming a spherical geometry for the AltC12 nanoparticles and neglecting their polydispersity, it is possible to estimate their mean radius from their specific surface area value and the mass fraction of AltC12 in the mixture (Eq. 5; Table 2). The value of 210 nm is consistent with the order of magnitude of the hydrodynamic radius determined by DLS and the sizes observed by Cryo-TEM (Fig. 5a—b), although the polydispersity of the suspension was not taken into consideration.

Once we compare the scattering intensities in the Porod region (q ≈ 10^{-3} – 10^{-2} $Å^{-1}$) of AltC18 nanoparticles generated from deuterated and non-deuterated THF, it is possible to observe that the scattering curve of the deuterated sample is above the scattering curve of the non-deuterated one, whereas both levels coincided in the AltC12 scattering data (Fig. 4b). Thus, the contrast variation in this case reveals that AltC12 nanoparticles have a different structure from AltC18 ones, where swelling of nanoparticles by the solvent should be considered. If applying the same reasoning as above, we would conclude that THF-d8-swollen AltC18 nanoparticles apparently show a higher interface density than THF-swollen ones. This observation suggests that the solvent is entrapped in the middle of the particles, showing inner interfaces when the solvent is deuterated and virtually no contrast when both solvent and polymer are hydrogenated. To test this hypothesis, we performed simultaneous fitting of both series of data using different assumptions for the location of solvent and polymer in the particles.

As SANS data do not show enough characteristic features to fix many structural parameters, and simple sphere models failed to explain the effect of deuterium labelling in the solvent, we strived to select the minimal model able to describe this feature. The best fitting model that describes the AltC18 scattering curves is the core-shell one, with solvent mixture located in the core. We believe that this model reveals the

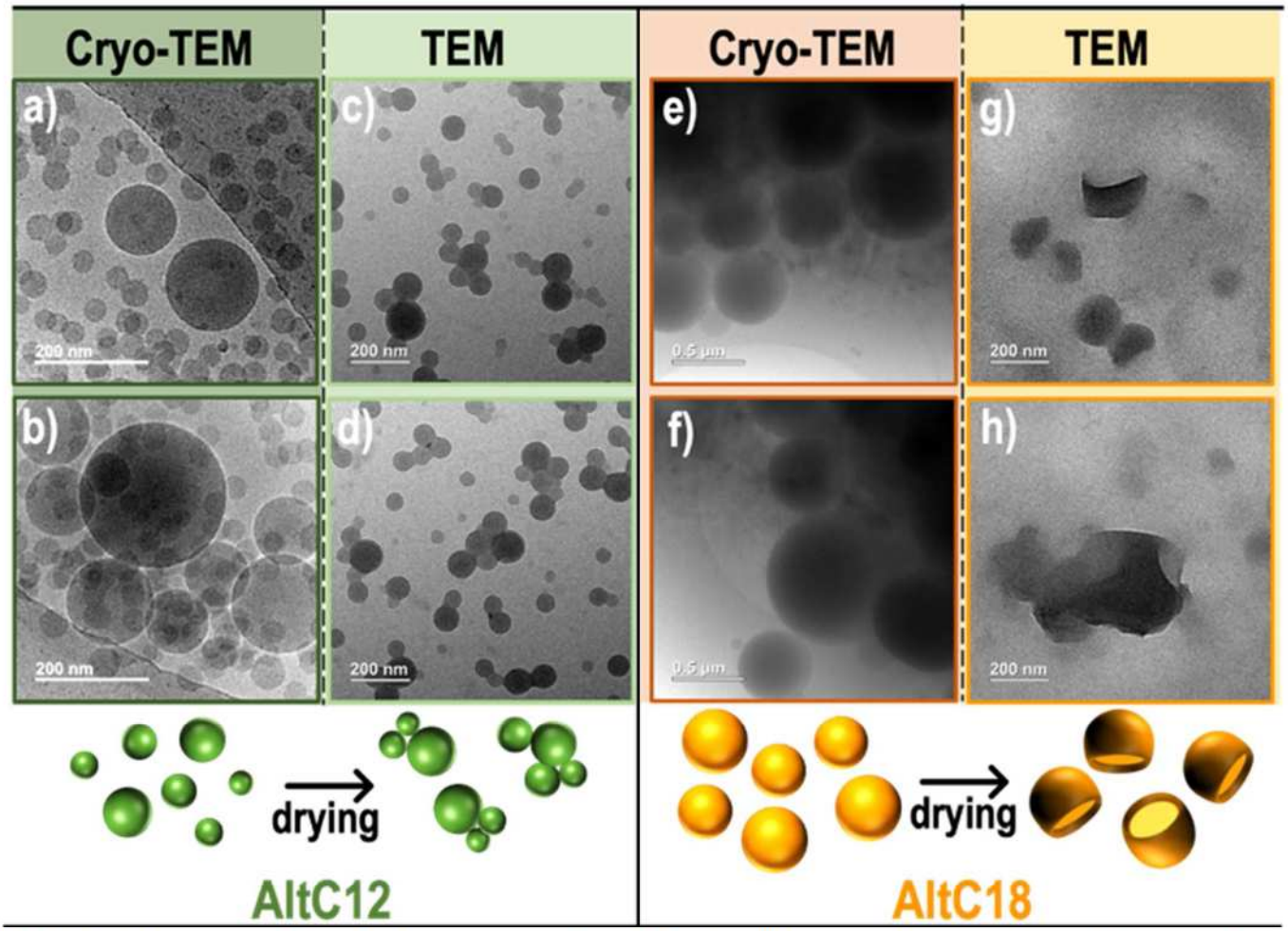

Fig. 5 Micrographs of copolymer nanostructures in suspension (copolymer/THF/H_2O ternary mixture) measured by Cryo-TEM: two regions are showed for AltC12 (a,b – scale of 200 nm at 40k magnification) and two regions are showed for AltC18 (e,f - scale of 0.5 µm at 10k magnification). Transmission electron micrographs (TEM) depict the nanostructures that are obtained after undergoing the drying process: two regions are showed for AltC12 (c,d – scale of 200 nm at 20k magnification) and two regions are showed for AltC18 (g,h – scale of 200 nm at 20k magnification). AltC12 nanoparticles resist the drying process while AltC18 ones outburst during solvent evaporation.

location of components in the structure, even though accurate determination of structural parameters and measurement of their distributions would require more data. In particular, we relied on a single fixed parameter (pinhole smearing fixed to 25%) to damp the oscillations of spherical form factors but a realistic model would have to take into account core and shell size variations as well as spectral width.

The constrained fitting of AltC18 SANS results in THF/D_2O and THF-*d*8/D_2O using the SasView software (Fig. S9) provides as fitting parameters the scattering length densities (SLDs) of the core and of the continuous aqueous phase in both mixtures (Table 2). Knowing that the SLDs of the core of the nanoparticles present values between the SLD of the copolymer (0.54 x $10^{10}cm^{-2}$, AltC18) and the solvent mixture, it is possible to infer that the core of AltC18 nanoparticles is constituted of a mixture of the copolymer and the solvents that are entrapped by a shell of AltC18.[46]

Considering that the SLD of the core can be calculated from the fractions of each component and their respective SLD, by solving a linear system, it is possible to determine the percentages of each component in the core of the nanoparticles (Supplementary Information). As a result, we find that the core is a mixture of about 11 % of water; 72 % of THF and 17 % of AltC18. The thickness of the copolymer shell and the radius of the nanoparticles are also fitting parameters and as shown in Table 2, the outermost radius of the core-shell nanoparticles is consistent with the value of R_H determined by DLS and with the sizes revealed by Cryo-TEM micrographs (Fig. 5e—f), considering that the polydispersity of the system was not taken into consideration.

Accordingly, one may infer that by tuning the amphiphilicity of the copolymer chains it is possible to achieve two different nanoparticle structures *via* the spontaneous ouzo effect (Scheme 2). For AltC12 (less lipophilic) the faster solvent diffusion to the aqueous medium leads to the formation of compact swollen nanoparticles, while for AltC18 (more lipophilic) the slower solvent diffusion and possible formation of an impermeable polymer skin leads to the formation of core-shell like structures, characterised by a shell of copolymer chains that entraps a core of copolymer and solvent mixture.

Finally, Cryo-TEM and TEM micrographs of AltC12 and AltC18 nanoparticles prepared in THF/H_2O aqueous suspensions (Fig. 5a—d and 5e—h, respectively) are in good agreement with the previous information derived from the

scattering techniques (DLS, SLS and SANS). In Fig. 5a—b, it is possible to identify the spherical nanoparticles assembled from AltC12 with the majority of sizes below the 200 nm scale. The Cryo-TEM micrographs show, respectively, two different regions where it is possible two distinguish two groups of nanoparticles, those with diameters less than 100 nm and a second group with bigger diameters. This result relates to the polydispersity index (PDI) of 0.17 found by DLS measurements. Also, TEM analysis show that AltC12 nanoparticles resist the capillary forces during the drying process. As depicted in Fig.5c—d, AltC12 nanoparticles have the same spherical aspect revealed by Cryo-TEM imaging.

As for AltC18 nanostructures, it is possible to see in Fig. 5e—f that they are bigger (scale of 0.5 μm) and, after drying, they outburst due to the solvent evaporation as detected in Fig. 5g—h. This result is in line with the hypothesis that AltC18 nanoparticles entrap the solvent in their structures. The polydispersity index found by DLS for AltC18 nanoparticles is of 0.04 which, for the different classes of dispersity,[47] indicates that they may be classified as monodisperse with narrow distribution of sizes (PDI from 0.0 to 0.1), also in agreement with the Cryo-TEM analysis.

Altogether, the results reported herein show that the protocol choice for nanoparticle preparation plays an important role on the self-assembled morphologies. Sequence controlled copolymers with one highly hydrophilic comonomer such as sodium maleate,[48] gluconamide[41] or quaternary ammonium[42] vinyl ethers tend to self-assemble into equilibrium colloidal structures such as micelles and vesicles upon solubilisation (binary mixtures), while using the solvent-shifting process the fast components interdiffusion leads to local chain supersaturation and mesoscopic colloidal nanoparticles are formed. By controlling the lateral lipophilicity, it is possible to prepare nanoparticles with different sizes and structures in submicron and nanoscales (< 500 nm), which is an interesting aspect considering applications where particle size should be in lower submicronic range as in the fields of pharmaceuticals, electronics and sensing.[2,14]

Conclusions

Sequence alternating copolymers consisting of vinyl phenol and alkyl-pendant maleimide units prepared *via* spontaneous radical copolymerization can be easily applied in aqueous medium thanks to the straightforward ouzo effect. The introduction of long alkyl chains into the maleimide units conferred tuneable lipophilicity, allowing the spontaneous formation of nanoparticles with different sizes and structures. During solvent-shifting to water, copolymer chains that are less lipophilic form smaller and slightly swelled nanoparticles as a consequence of a faster supersaturation process and solvent partition, while copolymer chains that are more lipophilic form core-shell like structures with a solvent mixture entrapped in the core. Also, structural analysis with light and neutron scattering techniques and Cryo-TEM/TEM imaging confirmed that the alternating copolymers self-assembled into stable nanoparticles in the submicronic size range. The ouzo diagram reported here is a meaningful source for the preparation of AB-alternating copolymer nanoparticles, as it shows the domain of occurrence of the nanostructures. This diagram could be a guide for preparation of matrix-type colloidal particles, in which a solute could be dissolved, entrapped, adsorbed, or chemically grafted for further technological applications of the alternating copolymers as in solute vectorisation.

Author Contributions

K.N. and M.O. investigated the chemical design and synthesis of alternated copolymers, H.T and F.T. investigated the phase diagram and structures and drafted the manuscript. J.M.G. contributed to microscopy analysis, S.A. contributed to data analysis methodology.

Conflicts of interest

There are no conflicts to declare.

Acknowledgements

We express our gratitude to Michel Cloitre for his support during light scattering experiments and for fruitful discussions and Lionel Porcar for his helpful contributions in SANS experiments and data analyses.

Funding

This project has received funding from the European Union's Horizon 2020 research and innovation programme under the Marie Skłodowska-Curie grant agreement No 754387. This work was also partially supported by the French National Research Agency (ANR) and the Japanese Science and Technology Agency (JST) (ANR-15-JTIC-0004) and Institut Laue-Langevin (ILL) Grenoble for provision of beamtime.[24]

References

1 Q. Shi, Y. Zhang, Z. Huang, N. Zhou, Z. Zhang and X. Zhu, *Polymer Journal*, 2020, **52**, 21–31.
2 Q. Xu, S. Li, C. Yu and Y. Zhou, *Chemistry – A European Journal*, 2019, **25**, 4255–4264.
3 J.-F. Lutz, J.-M. Lehn, E. W. Meijer and K. Matyjaszewski, *Nature Reviews Materials*, 2016, **1**, 1–14.
4 B. Klumperman, *Polym. Chem.*, 2010, **1**, 558–562.
5 J.-F. Lutz, M. Ouchi, D. R. Liu and M. Sawamoto, *Science*, 2013, **241**, 1238149.
6 K. Nishimori and M. Ouchi, *Chem. Commun.*, 2020, **56**, 3473–3483.
7 Y. Kametani, F. Tournilhac, M. Sawamoto and M. Ouchi, *Angewandte Chemie International Edition*, 2020, **59**, 5193–5201.
8 C. Solans, D. Morales and M. Homs, *Current Opinion in Colloid & Interface Science*, 2016, **22**, 88–93.
9 J. N. Israelachvili, *Intermolecular and Surface Forces*, Elsevier, California, 2011.
10 Z. Deng and S. Liu, *Polymer*, 2020, **207**, 122914.

11 C. E. Mora-Huertas, H. Fessi and A. Elaissari, *Adv Colloid Interface Sci*, 2011, **163**, 90–122.
12 H. Yabu, *Polymer Journal*, 2013, **45**, 261–268.
13 E. Cazares-Cortes, B. C. Baker, K. Nishimori, M. Ouchi and F. Tournilhac, *Macromolecules*, 2019, **52**, 5995–6004.
14 E. Busseron, Y. Ruff, E. Moulin and N. Giuseppone, *Nanoscale*, 2013, **5**, 7098.
15 M. Ueda, A. Hashidzume and T. Sato, *Macromolecules*, 2011, **44**, 2970–2977.
16 K. Nishimori, E. Cazares-Cortes, J.-M. Guigner, F. Tournilhac and M. Ouchi, *Polym. Chem.*, 2019, **10**, 2327–2336.
17 J. Aubry, F. Ganachaud, J.-P. Cohen Addad and B. Cabane, *Langmuir*, 2009, **25**, 1970–1979.
18 S. A. Vitale and J. L. Katz, *Langmuir*, 2003, **19**, 4105–4110.
19 H. Trevisan and C. A. Rezende, *Industrial Crops and Products*, 2020, **145**, 112105.
20 F. Ganachaud and J. L. Katz, *ChemPhysChem*, 2005, **6**, 209–216.
21 E. Aschenbrenner, K. Bley, K. Koynov, M. Makowski, M. Kappl, K. Landfester and C. K. Weiss, *Langmuir*, 2013, **29**, 8845–8855.
22 E. Lepeltier, C. Bourgaux and P. Couvreur, *Advanced Drug Delivery Reviews*, 2014, **71**, 86–97.
23 M. Beck-Broichsitter, J. Nicolas and P. Couvreur, *Nanoscale*, 2015, **7**, 9215–9221.
24 H. A. Almoustafa, M. A. Alshawsh, Z. Chik *International Journal of Pharmaceutics*, 2017, **533**, 275-284.
25 M. Beck-Broichsitter, *Int J Pharm*, 2016, **511**, 262–266.
26 W. J. Work, K. Horie, M. Hess and R. F. T. Stepto, *Pure and Applied Chemistry*, 2004, **76**, 1985–2007.
27 S. Rostami and D. J. Walsh, *Polymer Engineering & Science*, 1987, **27**, 315–323.
28 X. Yan, M. Delgado, J. Aubry, O. Gribelin, A. Stocco, F. Boisson-Da Cruz, J. Bernard and F. Ganachaud, *J. Phys. Chem. Lett.*, 2018, **9**, 96–103.
29 W. Schärtl, *Light Scattering from Polymer Solutions and Nanoparticle Dispersions*, Springer-Verlag, Berlin Heidelberg, 2007.
30 B. Hammouda, *Journal of Applied Crystallography*, 2010, **43**, 716–719.
31 F. Tournilhac, L. Porcar and H. Trevisan, DOI:10.5291/ILL-DATA.9-11-1967.
32 M. Shibayama, *Polym J*, 2011, **43**, 18–34.
33 I. Grillo, *Colloids and Surfaces A: Physicochemical and Engineering Aspects*, 2003, **225**, 153–160.
34 SasView, About SasView, https://sasview.github.io/about/, (accessed December 10, 2020).
35 I. Grillo, *L'actualité chimique*, 2005, **209**, 41-44.
36 P. Lucas, M. Vaysse, J. Aubry, D. Mariot, R. Sonnier and F. Ganachaud, *Soft Matter*, 2011, **7**, 5528.
37 C. Vauthier and K. Bouchemal, *Pharm Res*, 2009, **26**, 1025–1058.
38 M. Beck-Broichsitter, E. Rytting, T. Lebhardt, X. Wang and T. Kissel, *European Journal of Pharmaceutical Sciences*, 2010, **41**, 244–253.
39 V. Kumar and R. K. Prud'homme, *Chemical Engineering Science*, 2009, **64**, 1358–1361.
40 J. Chen, C. Yu, Z. Shi, S. Yu, Z. Lu, W. Jiang, M. Zhang, W. He, Y. Zhou and D. Yan, *Angew. Chem. Int. Ed.*, 2015, **54**, 3621–3625.
41 S. G. Fenimore, L. Abezgauz, D. Danino, C.-C. Ho and C. C. Co, *Macromolecules*, 2009, **42**, 2702–2707.
42 D. Wu, L. Abezgauz, D. Danino, C.-C. Ho and C. C. Co, *Soft Matter*, 2008, **4**, 1066–1071.
43 E. Niezabitowska, A. R. Town, B. Sabagh, M. D. M. Moctezuma, V. R. Kearns, S. G. Spain, S. P. Rannard and T. O. McDonald, *Nanoscale Adv.*, 2020, **2**, 4713–4721.
44 B. Hirzinger, M. Helmstedt and J. Stejskal, *Polymer*, 2000, **41**, 2883–2891.
45 D. Saha, F. Testard, I. Grillo, F. Zouhiri, D. Desmaele, A. Radulescu, S. Desert, A. Brulet, P. Couvreur and O. Spalla, *Soft Matter*, 2015, **11**, 4173–4179.
46 M. Cors, L. Wiehemeier, O. Wrede, A. Feoktystov, F. Cousin, T. Hellweg and J. Oberdisse, *Soft Matter*, 2020, **16**, 1922–1930.
47 Polydispersity-what does it mean for DLS and Chromatography,https://www.materials-talks.com/blog/2017/10/23/polydispersity-what-does-it-mean-for-dls-and-chromatography/, (accessed February 10, 2021).
48 K. Uramoto, R. Takahashi, K. Terao and T. Sato, *Polym J*, 2016, **48**, 863–867.